Title

Development of a compact explicit algebraic model for the turbulent heat fluxes and its application in heated rotating flows

Authors

Müller, H
Younis, BA
Weigand, B

Publication Date

2015-07-01

DOI

10.1016/j.ijheatmasstransfer.2015.03.059

Peer reviewed

International Journal of Heat and Mass Transfer 86 (2015) 880–889

Contents lists available at ScienceDirect

International Journal of Heat and Mass Transfer

journal homepage: www.elsevier.com/locate/ijhmt

Development of a compact explicit algebraic model for the turbulent heat fluxes and its application in heated rotating flows

H. Müller [a,*], B.A. Younis [b], B. Weigand [a]

[a] Institut für Thermodynamik der Luft- und Raumfahrt, Universität Stuttgart, 70569 Stuttgart, Germany
[b] Department of Civil & Environmental Engineering, University of California, Davis, CA 95616, USA

ARTICLE INFO

Article history:
Received 28 September 2014
Received in revised form 14 March 2015
Accepted 17 March 2015
Available online 9 April 2015

Keywords:
Scalar flux modeling
Turbine blade cooling
System rotation
Reynolds stress closure

ABSTRACT

The paper describes the development of a compact, non-linear model for the turbulent heat fluxes, and its application to heated flow in a rotating channel. The model was formulated by expanding the tensorial functional of dependent variables, and by applying certain simplifications to obtain an algebraic and explicit model that contains direct dependence on the rotational body forces, and on the gradients of mean velocity. The model was implemented into OpenFOAM, the open-source flow solver, and its performance was assessed in stationary wall-bounded and free heated flows, and in a heated channel with spanwise rotation. Comparisons with experimental data and with results from Direct Numerical Simulations show that the new model performs better than alternative closures.

1. Introduction

The aim of the research reported herein is to improve the prediction of the turbulent heat transfer in rotating passages. This problem is of immense practical importance as it occurs in several components of power-generation and propulsion systems. In turbine blades, for example, cold air is piped through internal passages to conduct heat away from the critical parts thereby allowing for operations at elevated temperatures. The cold air is typically bled from the compressor stage of the turbine and thus its flow into these passages represents a reduction in the system's overall efficiency. There is then a clear need to reduce the flow of cold air to the minimum level that is sufficient to allow for engine operation at the design temperature. The flow and heat transfer in such cooling systems are currently predicted by using the Reynolds averaged Navier–Stokes equations (RANS) together with the energy equation. This is mainly due to the fact that the high Reynolds numbers in such applications do not allow the use of the computationally more demanding Large-Eddy Simulations (LES) or Direct Numerical Simulations (DNS) in routine design calculations. Reviews of work in this area are given for example in [1,2]. Key to the ability to predict the flow in such systems by using RANS methods is the availability of a model for the turbulent heat fluxes that can be relied upon to yield results of acceptable engineering accuracy. At present, the default model for the turbulent heat fluxes is Fourier's law in which the heat fluxes are assumed to be proportional to the temperature gradients. Absent from this model is a dependence on the mean velocity gradients and on the details of the turbulence field. Such dependence is evident from inspection of the exact equations that govern the conservation of these fluxes (Eq. 1), and its absence from Fourier's law seriously diminishes its predictive reliability in heated rotating flows. An example of where this is the case is the flow in a straight channel which is rotated about a spanwise axis. This flow has been the subject of extensive experimental and numerical studies, the latter using both RANS approaches as well as DNS (e.g. [3–5]). It was found that the effects of spanwise rotation were to reduce the turbulent mixing on the suction side relative to the equivalent stationary flow, and to enhance it on the pressure side. When rotation is sufficiently strong, the flow relaminarizes on the suction side thereby significantly reducing the heat-transfer rate from that surface leading to the formation of local hot spots. These effects are not reproducible by any gradient-transport model that has not specifically modified in some ad hoc way. In what follows, we describe the development of an explicit, algebraic model for the turbulent heat fluxes, assess this model's performance in a number of benchmark heated shear flows, and report on the outcome of its application to the prediction of flow in a heated channel with spanwise rotation.

* Corresponding author at: Institut für Thermodynamik, Universität der Bundeswehr München, Werner-Heisenberg-Weg 39, 85577 Neubiberg, Germany.
E-mail addresses: hagen.mueller@unibw.de (H. Müller), bayounis@ucdavis.edu (B.A. Younis), bernhard.weigand@itlr.uni-stuttgart.de (B. Weigand).

http://dx.doi.org/10.1016/j.ijheatmasstransfer.2015.03.059
0017-9310/

Nomenclature

Latin letters

A	stress flatness parameter [–]
b_{ij}	turbulence anisotropy tensor [–]
II_b	second invariant of b_{ij} [–]
c_f	friction coefficient [–]
c_p	specific heat capacity at constant pressure [J/(kg K)]
H	channel half width [m]
k	turbulent kinetic energy [m^2/s^2]
Nu	Nusselt number [–]
p	pressure [Pa]
$p\prime$	fluctuating pressure [Pa]
P_{ij}	production of Reynolds stress [m^2/s^3]
P_k	production of turbulent kinetic energy [m^2/s^3]
Pe_t	turbulent Peclet number [–]
Pr	Prandtl number [–]
$\dot{q}_w$	wall heat flux [W/m^2]
Re	Reynolds number [–]
Re_t	turbulent Reynolds number [–]
Ro	rotation number [–]
S_{ij}	mean rate-of-strain tensor [1/s]
St	Stanton number [–]
U_b	channel bulk velocity [m/s]
u_i	fluctuating velocity component [m/s]
U_i	mean velocity component [m/s]
U_τ	friction velocity [m/s]
W_{ij}	vorticity tensor [1/s]
x_i	spatial coordinate [m]
$y+$	normalized wall distance [–]

Greek letters

α	heat transfer coefficient [$W/(m^2\ K)$]
γ	Thermal diffusivity [m^2/s]
δ_{ij}	Kronecker delta [–]
ϵ	dissipation of turbulent kinetic energy [m^2/s^3]
ϵ_{ij}	dissipation of Reynolds stress [m^2/s^3]
ϵ_{ijk}	alternating tensor [–]
ϵ_θ	dissipation of scalar variance [K^2/s]
θ	fluctuating temperature [K]
Θ	mean temperature [K]
Θ_b	channel bulk temperature [K]
Θ_τ	friction temperature [K]
λ	thermal conductivity [W/(m K)]
ν	kinematic viscosity [m^2/s]
ρ	density [kg/m^3]
τ_{ij}	Reynolds stress tensor [m^2/s^2]
τ_w	wall friction [N/m^2]
τ_θ	scalar fluctuation time scale [s]
Ω_i	angular velocity component [1/s]

2. Model development

The starting point in the development of the model for the turbulent heat fluxes is provided by the exact equations that describe their conservation. For an incompressible fluid in an inertial frame, these equations are obtained by multiplying the equation for $(\Theta+\theta)$ by u_i and the equation for (U_i+u_i) by θ, then by adding the two and time averaging the result to obtain:

$$\begin{aligned}\frac{\partial \overline{u_i\theta}}{\partial t}+U_k\frac{\partial \overline{u_i\theta}}{\partial x_k}=&\overbrace{-\overline{u_k u_i}\frac{\partial\Theta}{\partial x_k}}^{\mathbf{P}_{i\theta,1}}\overbrace{-\overline{u_k\theta}\frac{\partial U_i}{\partial x_k}}^{\mathbf{P}_{i\theta,2}}\overbrace{-2\epsilon_{ijk}\Omega_j\overline{u_k\theta}}^{\mathbf{P}_{i\theta,3}}\\&-(\gamma+\nu)\overline{\frac{\partial\theta}{\partial x_k}\frac{\partial u_i}{\partial x_k}}\\&-\frac{\partial}{\partial x_k}\left(\overline{u_k u_i\theta}+\overline{\frac{p'\theta}{\rho}}\delta_{ik}-\gamma\overline{u_i\frac{\partial\theta}{\partial x_k}}-\nu\overline{\theta\frac{\partial u_i}{\partial x_k}}\right)\\&-\overline{\frac{p'}{\rho}\frac{\partial\theta}{\partial x_i}}\end{aligned}\tag{1}$$

where ν and γ are respectively the fluid kinematic viscosity and molecular diffusivity, ρ is the fluid density, and p' is the fluctuating pressure.

The terms $P_{i\theta,1}$ and $P_{i\theta,2}$ represent, respectively, the rates at which the heat fluxes are generated by the interactions between the temperature field and the Reynolds stresses, and between the heat fluxes themselves and the mean shear. The term $P_{i\theta,3}$ arises when flow is subjected to system rotation around an arbitrary axis. Experimental data and results from DNS on stationary and rotating flows indicate that the production terms represent the largest contribution to the heat-flux balances and, as such, would exert most influence in determining the magnitude of these fluxes, and their response to changes in the turbulence structure and in the mean velocity field. An algebraic model for $\overline{u_i\theta}$ must therefore explicitly depend on the Reynolds stresses and the gradients of mean velocity, as well as on the gradients of mean temperature. The parameters of the functional relationship are immediately evident from Eq. (1) which suggests:

$$\overline{u_i\theta}=f_i(\overline{u_iu_j},S_{ij},W_{ij},\Theta_{,j},\epsilon_\theta,\tau_\theta)\tag{2}$$

where τ_θ is the time scale for the turbulent scalar fluctuations. S_{ij} and W_{ij} are, respectively, the mean rate-of-strain and the vorticity tensor:

$$S_{ij}=\frac{1}{2}\left(\frac{\partial U_i}{\partial x_j}+\frac{\partial U_j}{\partial x_i}\right)\tag{3}$$

$$W_{ij}=\frac{1}{2}\left(\frac{\partial U_i}{\partial x_j}-\frac{\partial U_j}{\partial x_i}\right)\tag{4}$$

Several alternative approaches are possible for developing an explicit model for the turbulent scalar fluxes that is consistent with Eq. (2) (e.g. [6,7]). Among these approaches is that of [8] who used the tensor representation theory developed in [9]. In this approach, a vector quantity $(\overline{u_i\theta})$ can be expressed in terms of basis vectors $\mathbb{V}_n$ (n = 1, ..., M) via a linear polynomial expansion which takes the form:

$$\overline{u_i\theta}=\sum_{n=1}^{M}\alpha_n\mathbb{V}_n\tag{5}$$

The basis vectors $\mathbb{V}_n$ are formed from the products of the symmetric (S_{ij},τ_{ij}) and the skew-symmetric (W_{ij}) tensors, and the vector $(\Theta_{,j})$ that appears in the functional relation. The procedure is explained in detail in reference [9], and the outcome for two-dimensional flows is given by:

$$\begin{aligned}-\overline{u_i\theta}=&\alpha_1\Theta_{,i}+\alpha_2\tau_{ij}\Theta_{,j}+\alpha_3S_{ij}\Theta_{,j}+\alpha_4\tau_{ik}\tau_{kj}\Theta_{,j}+\alpha_5S_{ik}S_{kj}\Theta_{,j}\\&+\alpha_6W_{ij}\Theta_{,j}+\alpha_7W_{ik}W_{kj}\Theta_{,j}+\alpha_8(S_{ik}W_{kj}+S_{jk}W_{ki})\Theta_{,j}\\&+\alpha_9(\tau_{ik}S_{kj}-\tau_{jk}S_{ki})\Theta_{,j}+\alpha_{10}(\tau_{ik}W_{kj}+\tau_{jk}W_{ki})\Theta_{,j}\end{aligned}\tag{6}$$

The α's in Eq. (6) are variable coefficients that can depend on all the tensor variables listed in the functional form, and their invariants.

It is by no means necessary to retain all the terms in Eq. (6) for the model to contain the required dependencies and yet be of value in the practical computation of turbulent flows. Thus if it is assumed that the anisotropies and turbulent time scales are sufficiently small to allow for a multilinear expansion, then terms that are quadratic in τ_{ij}, S_{ij} and W_{ij} can be neglected. Further, if the effects of the rotational and irrotational strains are in balance, then the terms in S_{ij} and W_{ij} may be combined to yield terms that contain the velocity gradients $U_{i,j}$.

With these assumptions, the following compact form is obtained:

$$-\overline{u_i\theta} = \alpha_1\Theta_{,i} + \alpha_2\tau_{ij}\Theta_{,j} + \alpha_3 U_{i,j}\Theta_{,j} + \alpha_9(\tau_{ik}U_{j,k} + \tau_{jk}U_{i,k})\Theta_{,j} \tag{7}$$

The formulation presented above does not take into account the effects of rotation on the turbulent heat fluxes. As indicated by Eq. (1), these effects must be explicitly accounted for in a model for the turbulent fluxes for it to be able to capture these effects. The most direct way to explicitly introduce the rotational effects is by recognizing that the proper expression for the mean velocity gradient tensor in a rotating frame is [10]:

$$\frac{\partial U_i}{\partial x_j} = \frac{\partial U_i}{\partial x_j} + \epsilon_{mji}\Omega_m \tag{8}$$

With this substitution in place, the complete model proposed in this study therefore takes the form:

$$-\overline{u_i\theta} = C_1^*\frac{k^2}{\epsilon}\frac{\partial\Theta}{\partial x_i} + C_2\frac{k}{\epsilon}\overline{u_iu_j}\frac{\partial\Theta}{\partial x_j} + C_3\frac{k^2}{\epsilon^2}\left(\overline{u_iu_k}\left(\frac{\partial U_j}{\partial x_k} + \epsilon_{jmk}\Omega_m\right) - \overline{u_ju_k}\left(\frac{\partial U_i}{\partial x_k} + \epsilon_{imk}\Omega_m\right)\right)\frac{\partial\Theta}{\partial x_j} \tag{9}$$

This model presented in Eq. (9) differs from that of reference [8] essentially by combining the isotropic and anisotropic terms in the mean velocity gradients on the basis that separation of the two does not significantly change the predictions while combining the two terms brings the distinct benefit of making the model more compact and thus easier to implement, and more robust to use in general-purpose computational methods. The values of the model coefficients would now be expected to be different from before in order to take into account the change in the balance of the remaining terms in Eq. (9). Determination of these constants is done by reference to the DNS results of Abe et al. [11] for a fully developed heated turbulent channel flow, and to experimental measurements obtained in heated plane and axisymmetric free jets. The values obtained thus are as follows:

In order to account for the wall-damping effects, the constant C_1 is made a function of the turbulent Peclet number in the manner suggested by [12]:

$$C_1^* = C_1\left(1 - e^{-A^\zeta Pe_t^\alpha}\right) \tag{10}$$

where $Pe_t = PrRe_t, \alpha = 0.2$ and $\zeta = 4$.

In summary, the model for the turbulent heat fluxes proposed here is given by Eq. (9) with the coefficients assigned the values given in Table 1. It is worth noting here that Fourier's law is represented by the first term in this equation – the remaining terms introduce the dependence on the details of the Reynolds structure via the $(\overline{u_iu_j})$ terms, and on the mean velocity gradients. Assessment of the performance of this model in stationary benchmark heated flows is presented next.

Table 1
Coefficients of scalar flux model.

C_1	C_2	C_3
0.03	0.21	−0.105

3. Preliminary model validation

3.1. A-priori testing

A-priori testing provides a reliable way to validate a new model since it does not involve the numerical solution of equations with its associated numerical uncertainties, nor does it involve input from other models that may themselves be deficient. Instead, results from Direct Numerical Simulations are used to obtain values of $\overline{u_i\theta}$ based on the model formulation. These values are then compared with the DNS results for the same correlations. This testing is performed here for the cases of a heated Couette flow and for a fully-developed flow in a heated channel.

Heated Couette flow.

The first case considered is that of a Couette flow with the upper wall moving at constant velocity U_w. The walls are semi-infinite and the flow is fully developed. Thus, the flow is one-dimensional and only dependent upon the wall distance. The temperature of the walls are kept constant, with the lower wall cooled and the upper wall heated. The configuration is shown in Fig. 1. Comparisons are made with the results from the DNS of Tsukahara et al. [13]. The wall Reynolds number ($Re_w = 4U_wH/\nu$, where U_w is the velocity of the moving wall and H is the channel half width) and the friction Reyonolds number ($Re_\tau = U_\tau H/\nu$, where U_τ is the friction velocity) is 25,600 and 181, respectively. The turbulent heat fluxes are non-dimensionalized with U_τ and Θ_τ and plotted over the wall distance y^+:

$$U_\tau = \sqrt{\frac{\tau_w}{\rho}} \qquad \Theta_\tau = \frac{\dot{q}_w}{\rho c_p U_\tau} \qquad y+ = U_\tau\frac{y}{\nu} \tag{11}$$

where τ_w denotes the absolute value of the friction at the wall, $\dot{q}_w$ the wall heat flux and c_p the specific heat capacity at constant pressure.

Fig. 2 compares the results of the present model with the available DNS data as well as with the model by [8]. The axial heat flux is well reproduced by both models. Differences can however be observed for the wall-normal heat flux component. In particular, the present model compares well with the reference near the wall while the model by [8] underpredicts the wall-normal turbulent transport. The difference can be attributed to the first term in the model Eq. 9 which is dominant in the viscous sublayer.

Heated turbulent channel flow.

Interest is confined to the fully-developed case with uniform heat flux applied at both walls. This arrangement was studied by Abe et al. [11] who performed DNS for a range of Reynolds number. Comparisons are made for two values of the channel Reynolds number ($Re = 4U_bH/\nu$, where U_b is the bulk velocity and H is the channel half width) viz. 28,248 and 82,882. The configuration is shown in Fig. 3. In both cases, the Prandtl number is $Pr = 0.71$. The results are non-dimensionalized by the friction velocity U_τ and the friction temperature Θ_τ.

Fig. 4 compares the turbulent heat fluxes as obtained from the present model and the model by [8] with the DNS data. As for the Couette flow, the new formulation predicts generally higher values and better captures the transition and sublayer. In the fully turbulent regime, minor differences can be observed between both models and the DNS of Abe et al. [11].

Both *a priori* tests are encouraging. Although more compact in its formulation, the present model performs equally good in the

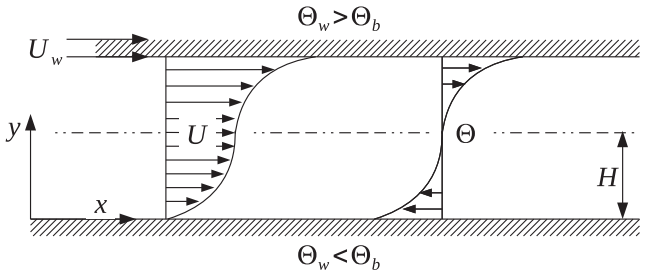

Fig. 1. Heated Couette flow.

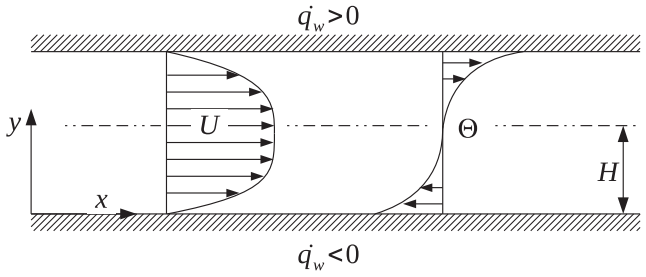

Fig. 3. Heated channel flow.

fully turbulent regime and slightly better in the transition and sublayer than its predecessor.

3.2. Two-dimensional flows

The model was also checked by actual computations against data from both wall-bounded and free shear flows. In these computations, the equations governing conservation of mass and momentum were solved using finite-volume discretisation. The effects of turbulence were accounted for by using a full Reynolds-stress transport model of turbulence. This level of closure requires the solution of a modeled differential transport equation for each of the Reynolds stresses, and one for the viscous dissipation rate. Of the various terms in the Reynolds-stress equations that require modeling, the one which has received most attention is the term that represents the redistribution of turbulence energy via the fluctuating pressure-strain correlations. Several models for these correlations have been put forward in the literature most of which can be expressed in the general form:

$$\Phi_{ij} = -(C_1\epsilon + C_1^* P_k)b_{ij} + C_2\epsilon\left(b_{ik}b_{kj} - \frac{1}{3}b_{kl}b_{kl}\delta_{ij}\right) + \left(C_3 - C_3^* II_b^{1/2}\right)kS_{ij} + C_4 k\left(b_{ik}S_{jk} + b_{jk}S_{ik} - \frac{2}{3}b_{kl}S_{kl}\delta_{ij}\right) + C_5 k(b_{ik}W_{jk} + b_{jk}W_{ik}) \quad (12)$$

Different models are obtained by assigning appropriate values to the coefficients in Eq. 12. The models chosen here are among those that have been extensively validated in a range of flows. They are the models of Launder et al. [14] (hereafter LRR-IP), the model of Speziale et al. [15] (hereafter SSG), and the model of Dafalias and Younis [16] (hereafter DY). The relevant model coefficients are listed in Table 2:

The LRR-IP model was used in conjunction with the Gibson and Launder proposals for a wall-damping function to represent the effects of a solid wall in modifying the fluctuating pressure field in its vicinity. Details of the complete model, and of the viscous dissipation rate equation used in all subsequent calculations can be found in [12,17].

Heated plane and axisymmetric free jets.

The computations of the heated plane and axisymmetric jets issuing into stagnant surroundings were performed using the EXPRESS computer code [18]. This is a boundary-layer code that solves the governing equations on a computational grid that adapts to the extent of the flow. Uniform distributions of velocity and turbulence were specified at the inlet plane and the computations were continued until the profiles became self similar.

Considering the plane free jet first, the predicted rate of spread (defined as the slope of the loci of the points where the axial velocity has fallen to half its local maximum value) obtained using the DY model was 0.101 which is in line with the measurements which obtain this parameter in the range 0.102–0.11. The predicted rate of growth of the thermal layer ($d\Theta_{0.5}/dx$) was 0.120 which contrasts well with the measured value of 0.128. In Fig. 5(a), a comparison is presented between the predicted and measured cross-stream distribution of mean temperature and both axial and vertical components of the heat fluxes. The profiles are plotted in self-similar coordinates where the subscripts m and ∞ refer to the local maximum and free-stream values, respectively. The measurements are those of Ramaprian and Chandrasekhara [19] and van der Hegge Zijnen [20]. For comparison, Fig. 5(a) also shows results obtained using the algebraic heat-flux model of [8] and those obtained using the usual eddy-diffusivity model (Fourier's law). The heat-flux component $\overline{v\theta}$, which is responsible for the lateral growth of the thermal layer, is reasonably well predicted by both algebraic models with the differences between the predictions and measurements being generally smaller than the differences between the two sets of measurements. In contrast, the eddy-diffusivity model underestimates the maximum value of this flux components and, consequently, underpredicts the rate of growth

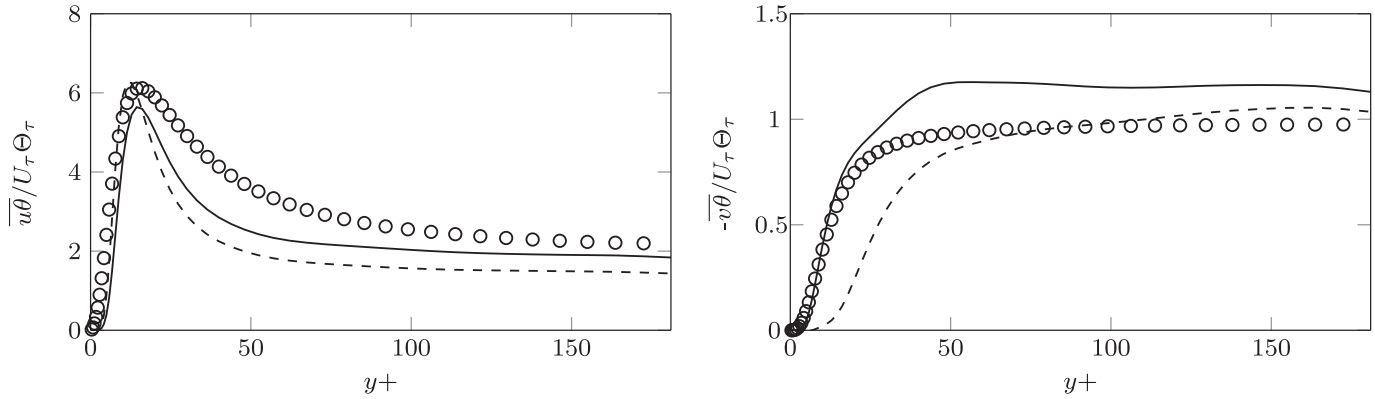

Fig. 2. Heated Couette flow: *A-priori* results of turbulent heat fluxes at $Re_w = 25,600$: — present model, –– model by [8], ◦ Tsukahara et al. [13].

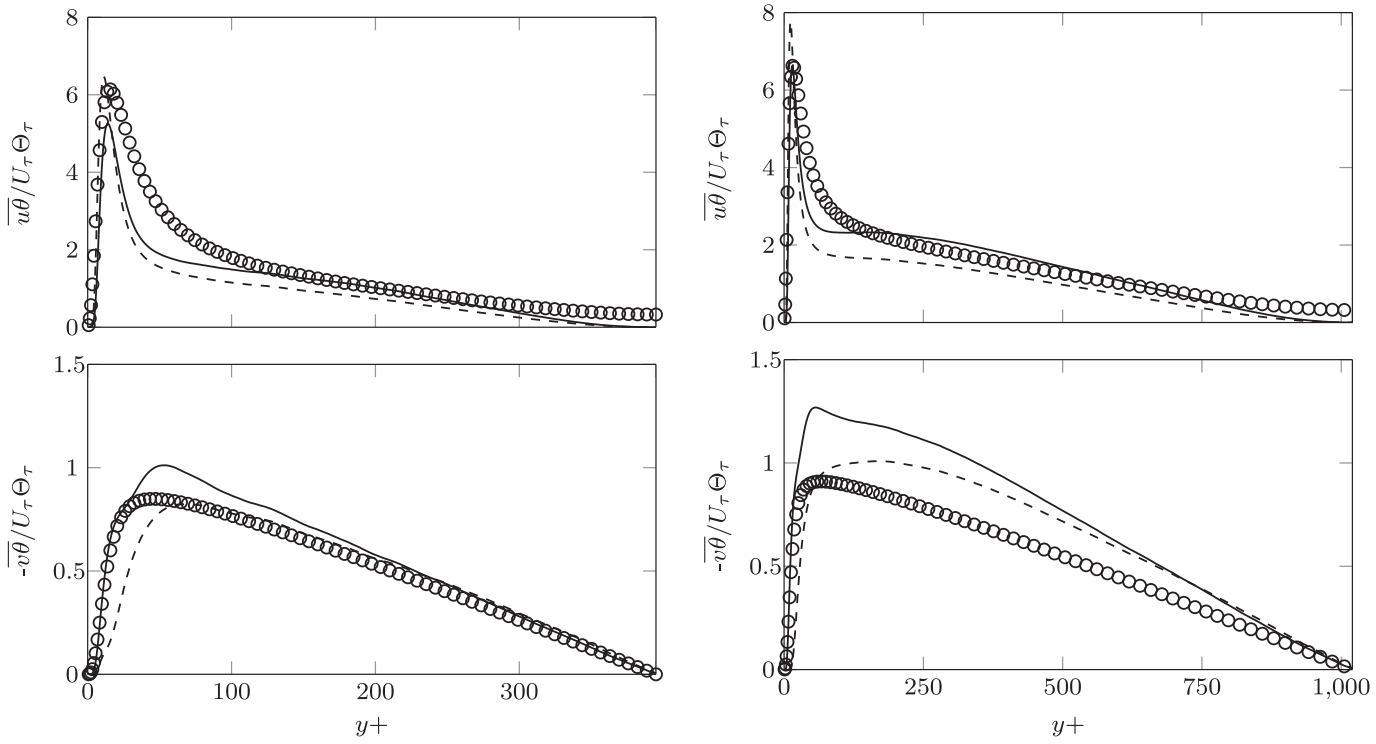

(a) $Re = 28,248$ (b) $Re = 82,882$

Fig. 4. Heated channel flow: *A-priori* results of turbulent heat fluxes: — present model, –– model by [8], ◦ Abe et al. [11].

of the thermal layer. Moreover, the same model obtains the axial heat flux component $\overline{u\theta}$ as zero while the two more complete algebraic closures correctly predict finite values that are of the same order as the vertical fluxes. In this particular shear-layer flow where turbulent transport is only significant in the cross-stream direction, the accurate prediction of $\overline{u\theta}$ is not especially important from a practical standpoint though this would not be the case in more complex flows.

Turning now to the axisymmetric heated jet, it is well established (e.g. [17]) that the standard Reynolds stress closures overestimate the jet spreading angle of the axisymmetric jet in stagnant surroundings by approximately 40%. In order to examine the heat-flux model performance in isolation of this result, the model constant $C_{\epsilon 1}$ which appears in the modeled equation for viscous dissipation is set in these calculation to 1.6. With this value, the predicted spreading rate is obtained with the DY model as 0.087 – a value which is consistent with experimental findings [21]. The predicted rate of growth of the thermal layer was 0.098. The predicted and measured cross-stream profiles of mean temperature and heat fluxes are presented in Fig. 5(b). Also presented there are the results obtained by Fourier's law, and by the model by [8]. As with the case of the plane jet, the present model and the model by [8] yield similar results for the profiles of mean temperature and the cross-stream heat-flux component which are broadly in agreement with the measurements of Chen and Rodi [22] and Antonia et al. [23]. The axial component of heat flux is not particularly well reproduced though the present model's results are distinctly better than those of [8].

Heated turbulent channel flow.

The performance of the model in wall-bounded applications was checked by performing computations for the flow in a heated channel. These computations are obtained with OpenFOAM[1]. This is an open-source computational software that solves the conservation equations for mass, momentum and thermal energy using finite volumes. Its open format makes it possible to modify and extend it by the addition of new models such as the one proposed here. In this test, the incompressible, pressure-based solution algorithm (SIMPLE [24]) was used to solve the governing equations. The Reynolds-averaged flow field in a channel with semi-infinite walls is two-dimensional and symmetric and thus only half of the channel height is discretized using 40 cells in the wall-normal direction and an axial grid spacing of $\Delta x = 1.5$ mm. The grid was systematically refined, with the non-dimensional wall distance of the grid nodes nearest to the wall kept at $y+ \approx 30$. Wall functions were used to bridge the near-wall region. At the inflow plane, uniform velocity and temperature profiles were specified. A constant heat flux was applied at the wall. The channel length-to-height ratio was 150 which is long enough to produce a fully-developed flow. The Reynolds number ($Re = 4U_bH/\nu$) was 82,882; the Prandtl number was set to 0.71.

Fig. 6 shows the present model's prediction for the normalized temperature and the turbulent heat fluxes in the fully-developed region of the channel. The result is compared with the model by [8], with Fourier's law as well as the DNS data of [11]. The underlying turbulence field is computed with the DY model. The temperature field and the wall normal turbulent heat flux is well predicted by all heat-flux models. Differences between them are distinct only for the axial component $\overline{u\theta}$, where the present model is closest to the DNS data.

The heat-flux model's ability to predict wall heat transfer is checked by comparison of the computed Nusselt number with correlations that are available in the literature. The Nusselt number was obtained from:

$$Nu = \frac{4H\alpha}{\lambda} = \frac{4H}{\Theta_w - \Theta_b}\left.\frac{\partial\Theta}{\partial y}\right|_w \tag{13}$$

[1] www.openfoam.com.

Table 2
Coefficients of alternative pressure-strain models.

Model	C_1	C_1^*	C_2	C_3	C_3^*	C_4	C_5
DY [16]	4.0	3.0	0	0.8	2.0	0.6	0
LRR-IP [14]	3.6	0	0	0.8	0	1.2	1.2
SSG [15]	3.4	1.8	4.2	0.8	1.3	1.25	0.4

Θ_b and Θ_w are the bulk and the wall temperatures, respectively. The temperature gradient is fixed by the uniform heat flux boundary condition and the wall temperature is calculated using appropriate wall functions. The simulations cover Reynolds numbers in the range 50,000–600,000. Fig. 7 compares the Nusselt number obtained with the present model with alternative closures. The Dittus–Boelter correlation ($Nu = 0.023\, Re^{0.8}\, Pr^{0.4}$) serves as a reference. The departure from the correlation increases at higher Reynolds number. In particular, the values obtained with Fourier's law are slightly lower than the correlation's prediction, whereas the values obtained with the model by [8] are higher. The present model yields the best agreement with the correlation.

The explicit appearance of the Reynolds stresses and the velocity gradient in the present model imposes a strong dependence of the turbulent heat flux on the turbulence closure which is used in the simulation. Thus, additional computations were performed using the LRR-IP and the SSG models. Table 3 shows the friction coefficient and the Nusselt number results for the different combinations of heat-flux and pressure-strain models at the Reynolds number 82,882. As expected, both the present heat-flux model and the model by [8] show a strong dependence on the turbulence field.

4. Application to the rotating channel

The heat-flux model is now applied to the flow in a heated channel that is rotated about its spanwise axis. The geometry is shown in Fig. 8. The effects of spanwise system rotation are to increase turbulent mixing on the pressure side, and to decrease it on the suction side. Simulations for such configurations were successfully performed using LES or DNS methods [25,26] where the Coriolis forces that originate from system rotation act mainly on

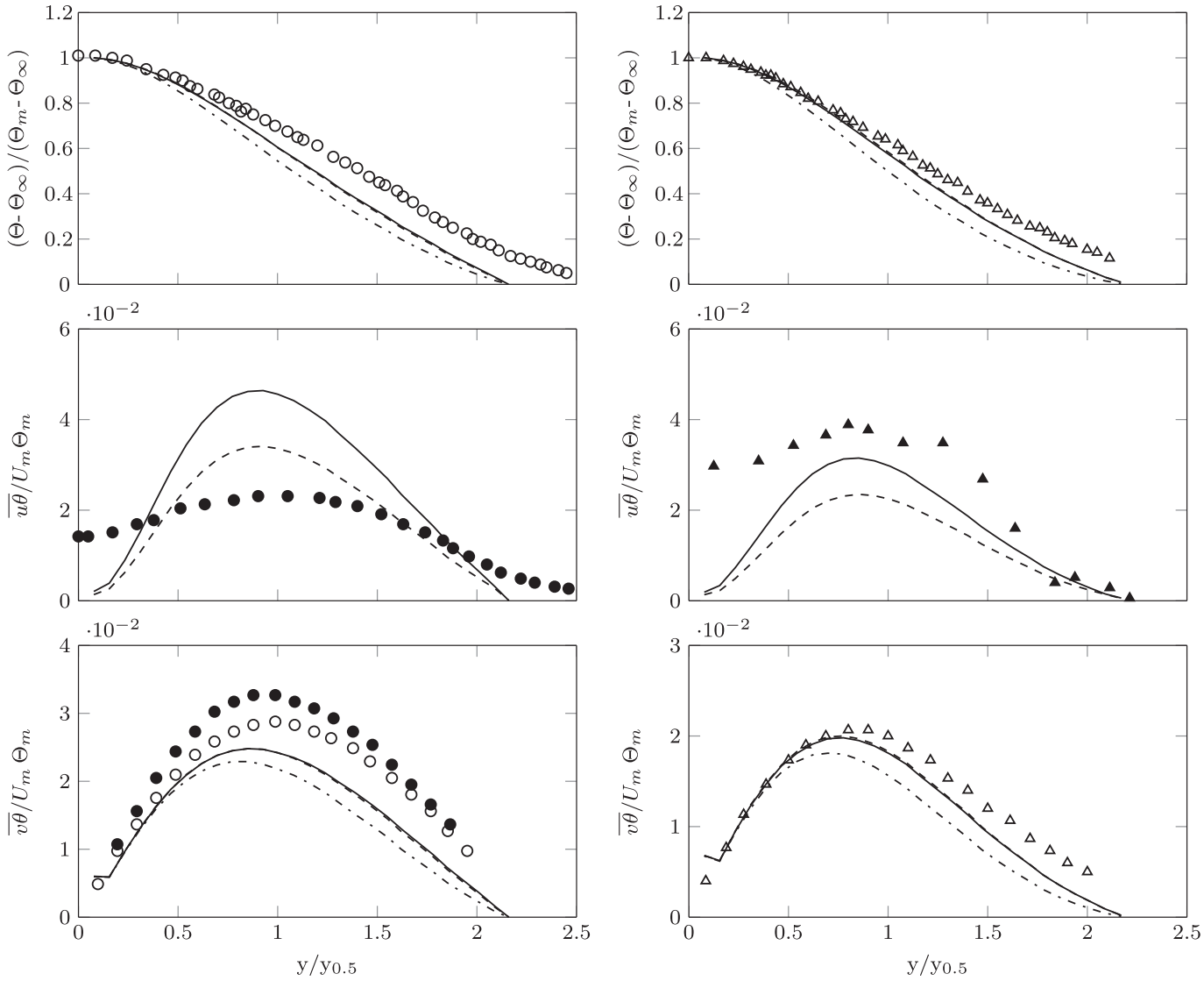

(a) Plane free jet (b) Axisymmetric free jet

Fig. 5. Free shear flows: Similarity profiles of mean temperature and turbulent heat fluxes. Data: ○, van der Hegge Zijnen [20]; •, Ramaprian and Chandrasekhara [19]; △, Chen and Rodi [22]; ▲, Antonia et al. [23]. Predictions: — present model, −− model by [8], – · – Fourier's law (0 for $\overline{u\theta}$).

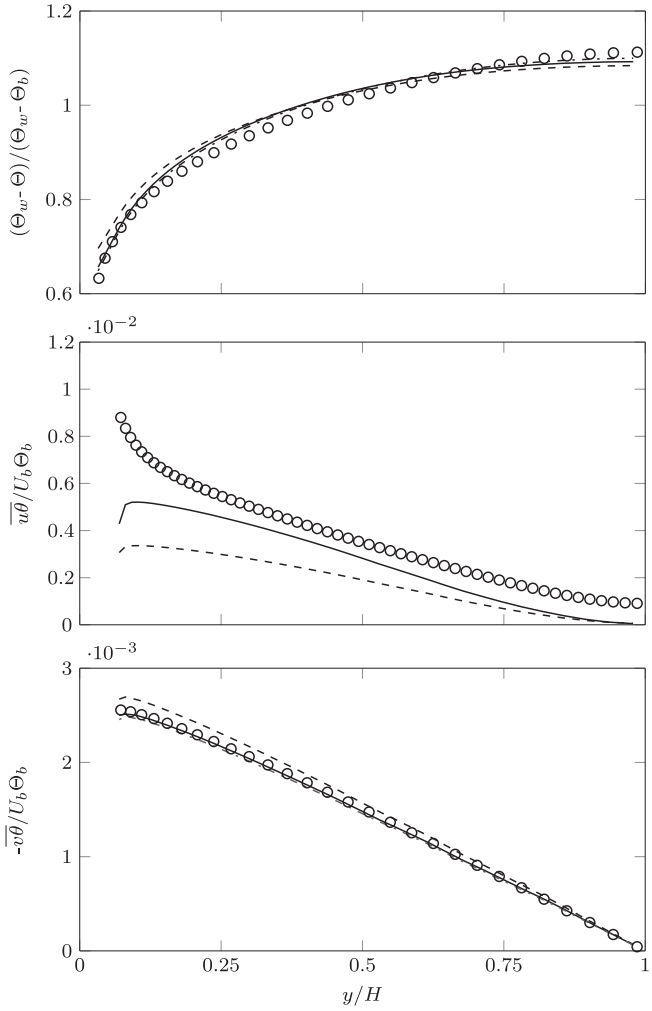

Fig. 6. Heated channel flow: Profiles of mean temperature and turbulent heat fluxes at $Re = 82,882$. The turbulence field is calculated using the DY model: — present model, −− model by [8], − · − Fourier's law (0 for $\overline{u\theta}$), ∘ Abe et al. [11].

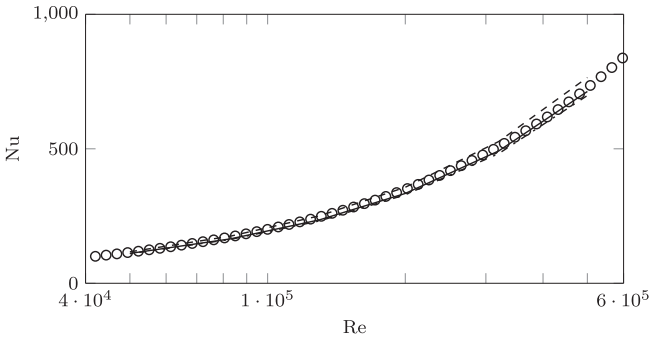

Fig. 7. Heated channel flow: Nusselt number over Reynolds number. The turbulence field is calculated using the DY model: — present model, −− model by [8], − · − Fourier's law, ∘ Dittus–Boelter correlation.

Table 3
Turbulent channel ($Re = 82,882$). Predicted Nusselt numbers and friction coefficient.

Model	c_f	Fourier's law *Nu*	Model by [8] *Nu*	Present model *Nu*
DY	4.87	163	175	165
LRR-IP	4.16	155	138	132
SSG	4.94	160	167	156
correlation	4.68	173	173	173

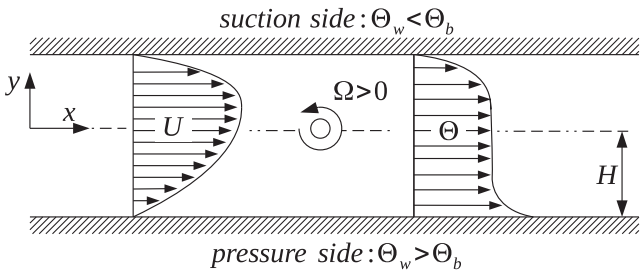

Fig. 8. Spanwise rotating channel flow.

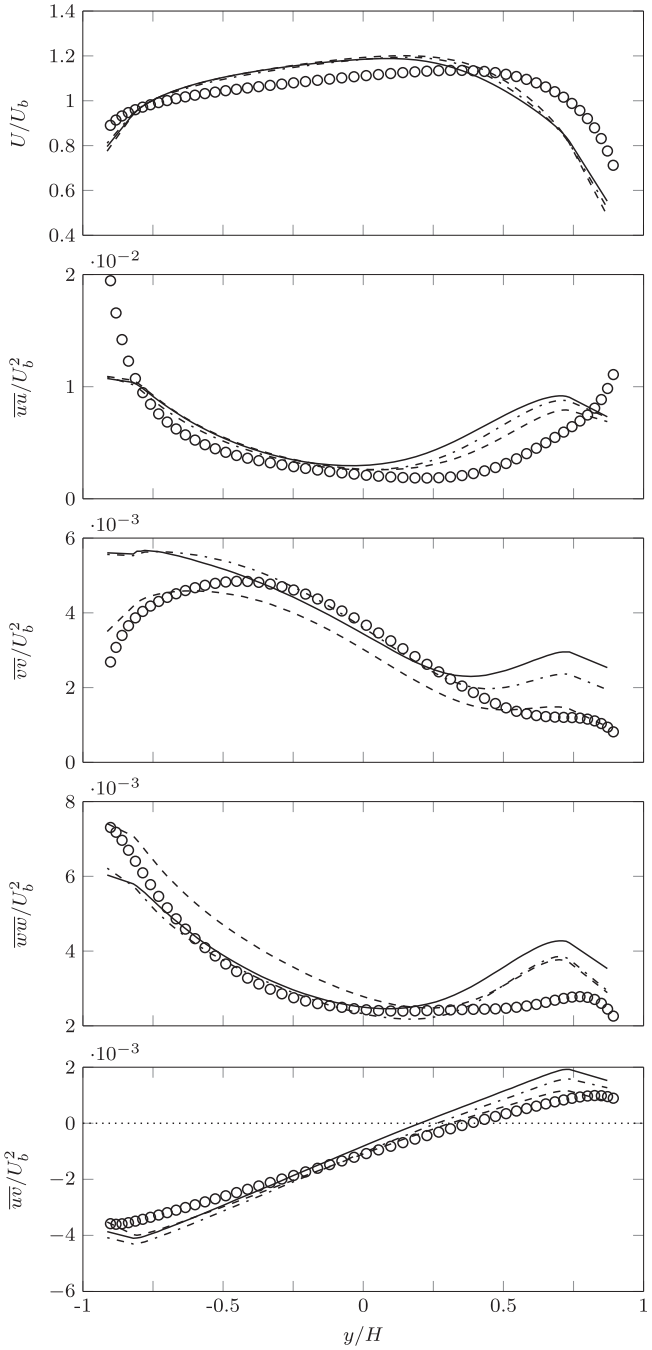

Fig. 9. Spanwise rotating channel: Profiles of mean velocity and turbulent Reynolds stresses at $Re = 21,522$ and $Ro = 0.137$: — DY, −− LRR-IP, − · − SSG, ∘ Wu and Kasagi [4].

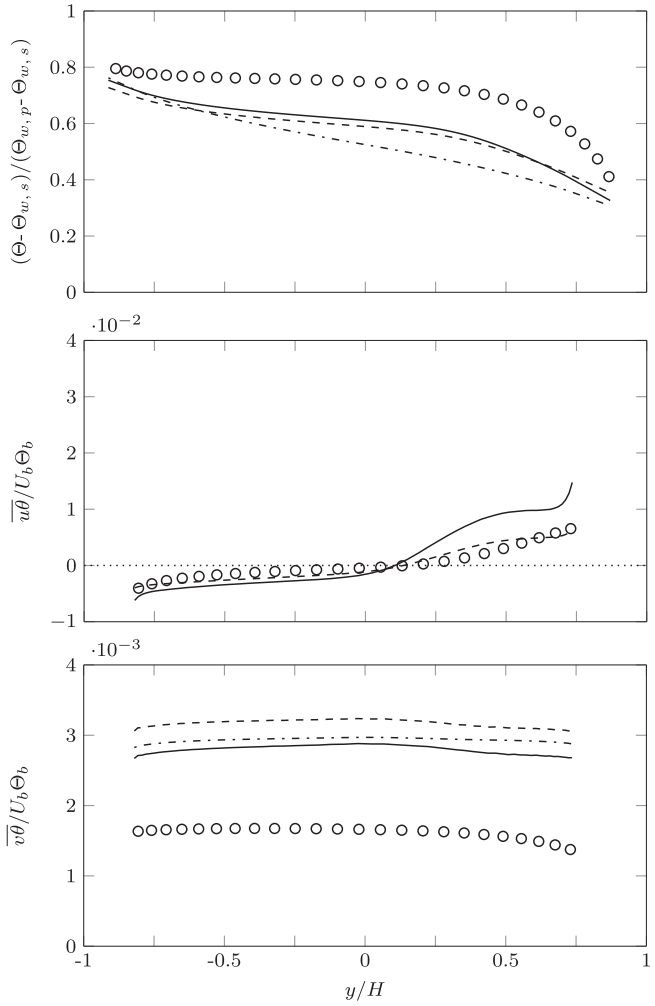

Fig. 10. Spanwise rotating channel: Profiles of mean temperature and turbulent heat fluxes at $Re = 21,522$ and $Ro = 0.137$. The turbulence field is calculated using the DY model: — present model, −− model by [8], − · − Fourier's law (0 for $\overline{u\theta}$), ∘ Wu and Kasagi [4].

Table 4
Friction coefficients ($\times 10^3$) and Nusselt numbers of the rotating channel flow at $Re = 21,522$ and $Ro = 0.137$.

Model			Fourier's law		Model by [8]		Present model	
	$c_{f,p}$	$c_{f,s}$	Nu_p	Nu_s	Nu_p	Nu_s	Nu_p	Nu_s
DY	6.77	3.55	41.2	34.9	51.8	37.4	48.6	33.5
LRR-IP	6.53	2.86	40.8	32	46.3	28.3	44.7	25.3
SSG	6.94	3.22	40	32.8	51.4	34.1	48.1	30.4
DNS [4]	8.27	3.72	58.4	26	58.4	26	58.4	26

the resolved flow scales and the influence of turbulence modeling is limited. However, using LES or DNS requires huge computational capacities and is only feasible for relatively low Reynolds numbers. It is thus desirable to obtain reliable results in the framework of Reynolds-averaged simulations where the effect of the Coriolis force on turbulence needs to be modelled carefully. An appropriate sensitization of the governing equations can be achieved by expressing the mean velocity gradient tensor in a rotating frame as shown by [10]. Furthermore, the production of Reynolds stress due to system rotation needs to be considered explicitly in the respective transport equation [27]. Since the present heat-flux model is sensitive to the turbulence field, we first examine the

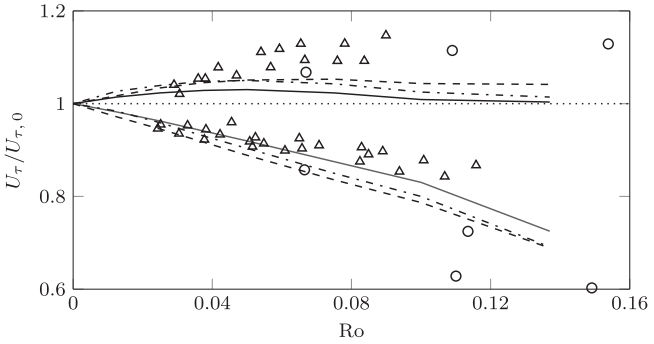

Fig. 11. Spanwise rotating channel: Wall friction velocity as function of rotation number at $Re = 21,522$: — DY, −− LRR-IP, − · − SSG, ∘ Johnston et al. [3] $23,400 < Re < 36,000$, △ Johnston et al. [3] $Re = 11,400$.

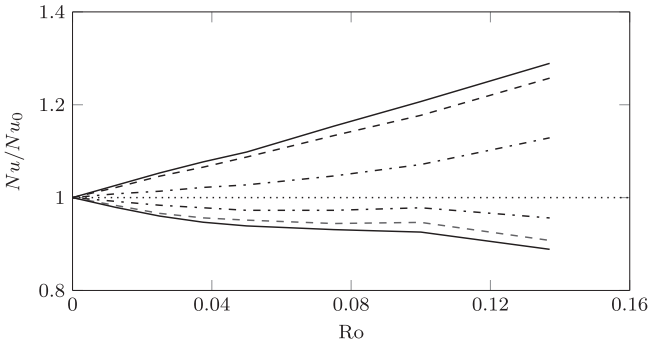

Fig. 12. Spanwise rotating channel: Nusselt number as function of rotation number at $Re = 21,522$. The turbulence field is calculated using the DY model: — present model, −− model by [8], − · − Fourier's law.

accuracy of Reynolds stress model and compare the three pressure-strain correlations that were previously used for the stationary channel flow, i.e., DY, LRR-IP and SSG.

The computations were again performed using the OpenFOAM code and the solution procedure was as described in Section 3.2. The rotating channel flow is two-dimensional but, in contrast to the previous simulations, not symmetric and the computational domain included the full channel height. 60 computational cells were used in the wall-normal direction and the axial grid spacing was $\Delta x = 1.5$ mm. The Reynolds number ($Re = 4U_bH/\nu$) was 21,522 and the dimensionless rotation number ($Ro = 4\Omega H/U_b$, where Ω is the rotational speed) was 0.137. The wall at the pressure side of the channel was heated, while the suction side was cooled, using a constant temperature boundary condition. In contrast to the stationary simulations, cyclic boundary conditions were used in the streamwise direction.

Fig. 9 shows the mean velocity and Reynolds stress profiles obtained with the various models for the pressure-strain correlations. Comparisons are made with the DNS result of Wu and Kasagi [4]. The various models are capable to varying degree of success in capturing the main characteristics of system rotation. Compared to the results for the stationary channel, the maximum velocity is shifted towards the suction side. This is in agreement with the DNS results. The section of constant velocity gradient in the channel center that is proportional to the rotation number [28] is well predicted. Furthermore, all closures produce an increase in the turbulence kinetic energy at the pressure and a decrease at the suction side. This agrees well with expectations, however, deviations with respect to the DNS are obvious especially near the wall. In particular, at the suction side of the channel all three models overpredict the turbulent stresses. This is probably due to partial laminarization effects which may be important at

$Ro = 0.137$ and which cannot be reproduced by the present closures. The experiments of Johnston et al. [3] indicate that laminarization may take place at even smaller rotation numbers. Comparing the different Reynolds stress models, we find that the SSG and DY exhibit broadly similar behavior. In what follows, the proposed heat-flux model is used in conjunction with the DY model.

Fig. 10 shows the temperature and turbulent heat flux obtained with the present model in rotational sensitized form (Eq. 9) in comparison with the DNS results of Wu and Kasagi [4]. Also shown are results obtained with the alternative closures of [8] and with a simple gradient transport approach (Fourier's law). The mean temperature is normalized with the wall temperature at the suction and at the pressure side ($\Theta_{w,s}$ and $\Theta_{w,p}$).

As mentioned above, spanwise system rotation increases turbulent mixing and thus turbulent heat transfer at the pressure side of the channel. In the current configuration, where the pressure side is heated and the suction is side cooled, the dimensionless bulk temperature Θ_b consequently increases with increasing rotational speeds. Note that the absolute value of the wall heat flux is the same at both walls once the flow field is fully developed. This effect is reproduced by the present model as well as by the model by [8] whereas the temperature field as obtained from Fourier's law shows little departure from the stationary-channel profile. The presence of the velocity gradient and the Reynolds stress components in the present model allows for the correct dependencies. When comparing the results with the DNS data, it is observed that none of the closures recovers the full increase in Θ_b. This is partly due to inadequacies in the performance of the Reynolds stress transport model which are apparent in the underprediction of the differences in turbulence kinetic energy between the suction and the pressure side of the channel (see Fig. 9). The difference is proportional to the bulk temperature increase since it determines the turbulent heat transfer. Fig. 10 also shows the predicted profiles of $\overline{u\theta}$ and $\overline{v\theta}$. Important features, such as the constant curve shape of $\overline{u\theta}$ and the different slope angles between pressure and suction side of $\overline{v\theta}$, are reproduced. A possible explanation for the offset of $\overline{v\theta}$ against the DNS data is the scaling with Θ_b.

The present heat-flux model's ability to predict the wall heat flux is further investigated by comparing the computed Nusselt number with the DNS result. Table 4 shows the results compared to that of the model by [8] and Fourier's law using the alternative pressure-strain correlations. The subscripts s and p refer to the suction and pressure sides, respectively. The results are in line with the previous observation that the difference in turbulent kinetic energy between the two walls is too small. Thus, the differences between Nu_p and Nu_s as well as between $c_{f,p}$ and $c_{f,s}$ are underpredicted by all models considered. However, the heat-flux models that explicitly incorporate the Reynolds stress tensor show a greater sensitivity to rotation, and better predict the observed increase in heat transfer rates at the pressure side, and the decrease at the suction side. Comparing the model of [8] with the present formulation, we find that the latter allows for a better prediction at the suction side at the cost of worse predictions at the pressure side. A clear dependence on the pressure-strain correlation is visible for both models, in particular the results obtained with the LRR-IP model are notably different from those obtained with SSG and DY. This dependence is absent in the results obtained with Fourier's law.

In order to evaluate the influence of the rotational speed on the wall heat transfer predictions, several simulations for rotation numbers in the range 0–0.137 were performed. The Reynolds number was kept constant at $Re = 21,522$.

First, the results from the various pressure-strain models closures are compared with the experiments of Johnston et al. [3]. Fig. 11 shows variation with the rotation number of the ratio of rotational to stationary friction velocity. The lower branch represents the friction velocity at the suction side of the channel, the upper one represents the pressure side. The sudden drop of U_τ that can be observed in the experiments at $Ro \approx 0.12$ corresponds to the beginning of laminarization. Beyond this threshold, computations with the present models are subject to increasing uncertainty since low Reynolds number effects are not included in the Reynolds-stress closure. However, the computational results match the experiments reasonably well, especially for smaller rotation numbers. Consistent with the previous results, the friction at the pressure side is slightly underpredicted, while the values at the suction side are in better agreement with the reference data. Unfortunately, the experimental scatter does not allow for a quantitative comparison of the different pressure-strain correlations.

The subsequent computations were performed with the DY model. Fig. 12 shows the normalized Nussult number. The results show that Fourier's law is least affected by the increase in rotational speed. This is consistent with the previous observation. Comparing the present model and that of [8], it can be observed that the new formulation yields slightly higher differences between pressure and suction side. Unfortunately, no reference data were available to assess the computational results quantitatively.

5. Concluding remarks

An alternative approach to modeling the turbulent heat fluxes has been developed by the use of results from tensor representation theory to obtain an explicit expression for the turbulent heat fluxes in terms of all the tensor quantities implied by the exact equations governing heat flux transport. A compact model that exhibits the correct dependencies and is suited to practical applications was deduced from the application of various assumptions one of which was that the isotropic and anisotropic terms that contain the gradients of mean velocity gradients can be combined without loss of realism. The result is an algebraic and explicit model for the turbulent heat fluxes which consists of three terms: one that is directly equivalent to gradient transport hypothesis and three others that contain products of the gradients of the mean velocity and the scalar. The values of the three coefficients in this model were determined by reference to results from Direct Numerical Simulations of standard benchmark heated shear flows. The new model was assessed both *a priori* and by actual computations against a wide range of two-dimensional heated flows and was found to perform satisfactorily. The model was then extended for use in a rotating frame of reference and was applied to the flow in a heated channel which is rotated about its spanwise axis. Comparisons with experimental and with DNS data at different rotation and Reynolds numbers showed that the present model predicts the main effects of rotation fairly well. In particular, an increase in the heat-transfer rate from the pressure side, and a decrease at the suction side was obtained. This represents a considerable improvement over the widely-used Fourier's law which lacks dependence on rotational parameters. Shortcomings were identified at high rotation numbers where flow relaminarization occurs but these can only be resolved once Reynolds-stress transport closures that can account for this phenomenon become available.

Acknowledgments

The financial support provided by the Hermann–Reissner–Stiftung and the Erich–Becker–Stiftung is gratefully acknowledged.

Table A.5
Sensitivity to heat-flux model coefficients.

		$C1$		$C2$		$C3$	
% Change in coefficient		+10%	−10%	+10%	−10%	+10%	−10%
Plane Jet: $d\Theta_{0.5}/dx$		+1.6%	0%	+4.1%	−1%	+0.5%	−0.5%
Round Jet: $d\Theta_{0.5}/dx$		+1.1%	+3%	+4.1%	−0.5%	+0.5%	+0.5%
Stationary channel: Nu		+0.43%	−0.43%	+2.79%	−3.04%	0%	0%
Rotating channel:	Nu_p	+0.39%	−0.39%	+2.98%	−3.28%	−0.33%	+0.25%
	Nu_s	+0.66%	−0.69%	+4.13%	−4.63%	+0.87%	−0.76%

Appendix A. Sensitivity study

In Section 2, it was mentioned that the values of the various coefficients in the heat-flux model were determined by reference to DNS and experimental results from benchmark wall-bounded and free flows. The quoted values offer the best fit between the target distributions of heat-flux components and those obtained from the model equations. In the interest of model robustness, the principal coefficients were assigned constant values rather than be made to depend in an elaborate manner on various turbulence parameters. The result is a set of values that yields a reasonably good fit for a wide range of flows. Table A.5 shows the sensitivity of the model predictions to ±10% change in each of the three coefficients. The results show that the bulk thermal parameters of the rate of spread of the thermal layer ($d\Theta_{0.5}/dx$) and the Nusselt number including on both the pressure and suction sides of the rotating channel depend only weakly on such large variations in the model coefficients.

References

[1] B. Weigand, K. Semmler, J. von Wolfersdorf, Gas turbine heat transfer and cooling technology, Ann. N. Y. Acad. Sci. 934 (2001) 179–193.
[2] J.C. Han, S. Dutta, S. Ekkad, Heat Transfer Technology for Internal Passages of Air-Cooled Blades for Heavy-duty Gas Turbines, CRC Press, 2012.
[3] J.P. Johnston, R.M. Halleen, D.K. Lezius, Effects of spanwise rotation on the structure of two-dimensional fully-developed turbulent channel flow, J. Fluid Mech. 56 (3) (1972) 533–557.
[4] H. Wu, N. Kasagi, Turbulent heat transfer in a channel flow with arbitrary directional system rotation, Int. J. Heat Mass Transfer 47 (21) (2004) 4579–4591.
[5] R. Kristoffersen, H.I. Andersson, Direct simulations of low Reynolds number turbulent flow in a rotating channel, J. Fluid Mech. 256 (1993) 163–197.
[6] M.M. Rogers, N.N. Mansour, W.C. Reynolds, An algebraic model for the turbulent flux of a passive scalar, J. Fluid Mech. 203 (1989) 77–101.
[7] R. Rubinstein, J. Barton, Renormalization group analysis of anisotropic diffusion in turbulent shear flows, Phys. Fluids A3 (1991) 415–421.
[8] B.A. Younis, C.G. Speziale, T.T. Clark, A rational model for the turbulent scalar fluxes, Proc. R. Soc. 461 (2005) 575–594.
[9] G.F. Smith, Constitutive Equations for Anisotropic and Isotropic Materials, Newnes, North-Holland, 1994.
[10] B.A. Younis, B. Weigand, F. Mohr, M. Schmidt, Modeling the effects of system rotation on the turbulent scalar fluxes, ASME J. Heat Transfer 132 (2010). 051703-051703-14.
[11] H. Abe, H. Kawamura, Y. Matsuo, Surface heat-flux fluctuations in a turbulent channel flow up to Re=1020 with Pr=0.025 and 0.71, Int. J. Heat Fluid Flow 25 (2004) 404–419.
[12] B.A. Younis, B. Weigand, S. Spring, An explicit algebraic model for turbulent heat transfer in wall-bounded flow with streamline curvature, ASME J. Heat Transfer 129 (2007) 425–433.
[13] T. Tsukahara, H. Kawamura, K. Shingai, DNS of turbulent Couette flow with emphasis on the large-scale structure in the core region, J. Turbul. 7 (2006).
[14] B.E. Launder, G.J. Reece, W. Rodi, Progress in the development of a Reynolds-stress turbulence closure, J. Fluid Mech. 68 (3) (1975) 537–566.
[15] C.G. Speziale, S. Sarkar, T.G. Gatski, Modelling the pressure strain correlation of turbulence: an invariant dynamical systems approach, J. Fluid Mech. 227 (1991) 245–272.
[16] Y.F. Dafalias, B.A. Younis, Objective model for the fluctuating pressure-strain-rate correlations, J. Eng. Mech. 135 (2009) 1006–1014.
[17] B.A. Younis, T.B. Gatski, C.G. Speziale, Assessment of the SSG pressure–strain model in free turbulent jets with and without swirl, ASME J. Fluids Eng. 118 (1996) 800–809.
[18] B.A. Younis, EXPRESS: Accelerated parabolic reynolds stress solver, City University, London Hydraulics Section Report HDBAY1, 1996.
[19] B.R. Ramaprian, M.S. Chandrasekhara, Study of vertical plane jets and plumes, IIHR Report no. 257, University of Iowa, USA, 1983.
[20] B.G. van der Hegge Zijnen, Measurement of the velocity distribution in a plane turbulent jet of air; measurement of the distribution of heat and matter in a plane turbulent jet of air, Appl. Sci. Res, A7 (4) (1958) 256–292.
[21] W. Rodi, The prediction of free turbulent boundary layers by use of a two-equation model of turbulence (Ph.D. thesis), University of London, 1972.
[22] C.J. Chen, W. Rodi, Vertical Turbulent Buoyant Jets: A Review of Experimental Data, Pergamon, Oxford, 1980.
[23] R.A. Antonia, A. Prabhu, S.E. Stephenson, Conditionally sampled measurements in a heated turbulent jet, J. Fluid Mech. 72 (3) (1975) 455–480.
[24] J.H. Ferzinger, M. Peric, Computational Methods for Fluid Mechanics, 2001.
[25] D.K. Tafti, S.P. Vanka, A numerical study of the effects of spanwise rotation on turbulent channel flow, Phys. Fluids 3 (4) (1991) 642–656.
[26] U. Piomelli, J. Liu, Large eddy simulation of rotating channel flows using a localized dynamic model, Phys. Fluids 7 (4) (1995) 839–848.
[27] B.E. Launder, D.P. Tselepidakis, B.A. Younis, A second moment closure study of rotating channel flow, J. Fluid Mech. 183 (1987) 63–75.
[28] Y. Nagano, H. Hattori, Direct numerical simulation and modelling of spanwise rotating channel flow with heat transfer, J. Turbul. 4 (10) (2003) 1–15.